



OPEN

Mid-infrared supercontinuum-based Fourier transform spectroscopy for plasma analysis

R. Krebbers¹, N. Liu^{1,2}, K. E. Jahromi¹, M. Nematollahi¹, O. Bang^{3,4,5}, G. Woyessa³, C. R. Petersen^{3,4}, G. van Rooij^{6,7}, F. J. M. Harren¹, A. Khodabakhsh^{1✉} & S. M. Cristescu¹

Broadband mid-infrared (MIR) spectroscopy is a well-established and valuable diagnostic technique for reactive plasmas. Plasmas are complex systems and consist of numerous (reactive) types of molecules; it is challenging to measure and control reaction specificity with a good sensitivity. Here, we demonstrate the first use of a novel MIR supercontinuum (SC) source for quantitative plasma spectroscopy. The SC source has a wide spectral coverage of 1300–2700 cm⁻¹ (wavelength range 3.7–7.7 μm), thus enabling broadband multispecies detection. The high spatial coherence of the MIR SC source provides long interaction path lengths, thereby increasing the sensitivity for molecular species. The combination of such a SC source with a custom-built FTIR spectrometer (0.1 cm⁻¹ spectral resolution) allows detection of various gases with high spectral resolution. We demonstrate its potential in plasma applications by accurate identification and quantification of a variety of reaction products (e.g. nitrogen oxides and carbon oxides) under low-pressure conditions, including the molecular species with overlapping absorbance features (e.g. acetone, acetaldehyde, formaldehyde, etc.).

One of the most promising emerging methods for reducing carbon dioxide (CO₂) emissions in chemical industrial processes is plasma-based gas conversion¹. This is particularly of interest for the conversion of two common greenhouse gasses, CO₂ and methane (CH₄) into carbon monoxide (CO) and hydrogen (H₂), also known as syngas^{2,3}. Although traditional (catalytic) pyrolysis and dry reforming methods are considered efficient ways to produce syngas and oxygenates from CO₂ and CH₄, high temperatures and pressures are usually required^{4–6}. To meet these requirements, the energy is largely supplied by burning fossil fuels, which is therefore accompanied by high CO₂ emissions. Compared to thermal methods, discharges can be powered by fully-sustainable green energy, avoiding CO₂ release^{1,7–12}. However, the plasmas formed in electric discharges are complex systems, consisting of numerous (reactive) species, and it is a challenge to control its reaction specificity. Therefore, it is of great importance to develop a detection system with good sensitivity and specificity to analyze the reaction products from the discharge for different plasma conditions (e.g., different feed gases, electric discharge power and mixing ratios).

The preferred analytical method for characterizing reaction products of an electric discharge is absorption spectroscopy^{13–15}, since it can combine high sensitivity and selectivity with excellent time resolution. The mid-infrared (MIR) wavelength region (2.5–25 μm) is of particular interest to the spectroscopy community, as many molecular gas species exhibit strong and unique absorption features in this region. Therefore, several different types of MIR sources are used for plasma diagnostics, such as MIR thermal sources (lamps)^{15,16}, tunable diode lasers¹⁴, Quantum Cascade Lasers (QCLs)^{17–19}, Interband Cascade Lasers (ICLs)²⁰ and optical frequency

¹Life Science Trace Detection Laboratory, Department of Analytical Chemistry and Chemometrics, Institute for Molecules and Materials, Radboud University, 6525 AJ Nijmegen, the Netherlands. ²Laser Spectroscopy and Sensing Laboratory, School of Physics and Materials Science, Anhui University, Hefei 230601, China. ³DTU Fotonik, Department of Photonics Engineering, Technical University of Denmark, 2800 Kgs. Lyngby, Denmark. ⁴NORBLIS ApS, Virumgade 35D, 2830 Virum, Denmark. ⁵NKT Photonics A/S, Blokken 84, 3460 Birkerød, Denmark. ⁶DIFFER - Dutch Institute for Fundamental Energy Research, De Zaale 20, 5612AJ Eindhoven, The Netherlands. ⁷Faculty of Science and Engineering, Maastricht University, Paul Henri Spaaklaan 1, 6229 GS Maastricht, The Netherlands. ✉email: A.Khodabakhsh@science.ru.nl

combs^{21,22}. While narrowband lasers, i.e., tunable diode lasers, ICLs, and QCLs, are well suited for sensitive detection of a specific molecule, they lack the ability to easily detect different types of molecules simultaneously.

Broadband absorption techniques, on the other hand, can detect and identify multiple species simultaneously, as is the case for the classical Fourier Transform InfraRed (FTIR) spectrometers, based on IR lamps²³. However, the omnidirectionality and divergence of light from these sources limits the optical interaction path length with the gas sample species. Moreover, the low spectral brightness of these sources requires the spectrum to be averaged over longer periods to achieve an acceptable signal-to-noise ratio (SNR), especially for high spectral resolution measurements.

Optical frequency combs overcome these limitations but have (with some notable exceptions²⁴) a relatively narrow spectral coverage. Furthermore, their high price and technical complexity limit their widespread use by end-users in real-life applications.

MIR supercontinuum (SC) sources are very suitable for broadband absorption spectroscopy, as they provide high spatial coherence, high spectral brightness, and ultra-broadband spectral coverage, outperforming conventional thermal sources and even some synchrotrons^{25–28}. SC sources have demonstrated powerful capabilities in emitting in the visible and near-infrared range using silica fibers. Sources emitting up to 4 μm using fluoride fibers have become commercially available in recent years²⁹. Several applications for these type of SC sources have been demonstrated, such as absorption spectroscopy with high sensitivity and selectivity for simultaneous measurement of multiple compounds³⁰, spectroscopic standoff detection³¹, or optical coherence tomography in the MIR range providing real-time and high-resolution images^{32,33}. Current developments in MIR SC sources extend the spectral range of the source beyond 4 μm to cover a larger part of the MIR fingerprint region³⁴. Applications in absorption spectroscopy³⁵ and hyperspectral imaging^{36,37} have been demonstrated for these highly experimental, new sources. Moreover, as the technology matures, this type of MIR SC sources is expected to be used for compact and cost-effective air quality sensor networks³⁸.

SC sources in the visible and near-infrared wavelength region have been previously used for plasma diagnostics³⁹, but to our knowledge, this report is the first demonstration of plasma diagnostics using a MIR SC source. Here, we demonstrate the advantages of MIR SC sources as broad spectral coverage (3.7–7.7 μm) and high sensitivity, achieved by the long optical path length of the spatially coherent beam.

Results

Experimental setup. The developed spectroscopic system consists of the MIR SC source, whose beam transmits through a multipass cell (MPC) containing the products of the plasma reaction at a low pressure. The transmitted beam is sent towards a custom-built Fourier Transform Spectrometer (FTS) with a spectral resolution of 0.1 cm^{-1} (3 GHz), allowing detection of narrow molecular absorption lines of gas species at a low pressure. Outside the MPC, the SC beam path was shielded and purged continuously with N_2 gas. The experimental setup is presented in Fig. 1. The light source is a newly developed, fiber-coupled MIR SC source (DTU Fotonik, average power ~ 86 mW, pulse duration ~ 0.5 ns, repetition frequency 3 MHz⁴⁰). The MPC has a 31.2 m effective interaction length (Thorlabs, HC30L/M-M02) and is connected to the discharge cell, such that the reaction products of the plasma are sent to the MPC for interaction with the SC beam. The custom-built FTS has been demonstrated and discussed in detail in our previous work³⁵. A brief description is presented in the Methods section, as well.

Source characterization. The spectral coverage of the MIR SC source was characterized with the FTS system by sending the SC light through the MPC under vacuum ($< 10^{-3}$ bar). The resulting power spectral density is shown in Fig. 2a and covers the spectral region between 1300 and 2700 cm^{-1} (3.7–7.7 μm). While most of the spectral power is between 1700 and 2100 cm^{-1} , spectroscopy in the other wavelength ranges is still feasible with high SNR, due to the high average power of the MIR SC source and sensitive photodetectors. Highly absorbing water (H_2O) and CO_2 lines can be observed in the spectrum, despite the measurement being performed under vacuum conditions. In Fig. 2a, the etalon fringes are also visible in the spectrum due to the partial overlap of the SC spots of the consecutive reflections on the MPC mirrors. However, the measured absorbance spectrum is not affected as the etalon fringes are stable and are canceled out by normalizing the sample spectra by the background spectra³⁵. The simulated spectral line intensities of the relevant species from the HITRAN2020 database⁴¹ between 1300 and 2500 cm^{-1} are shown in Fig. 2b. Due to the overlap of the absorption lines, a low pressure (16.5 mbar) and a high spectral resolution (3 GHz/0.1 cm^{-1}) are required to distinguish between the absorption lines.

System validation. To initially evaluate the performance of the MIR SC FTS-based system, we measured the spectrum of a gas mixture of 495 ppm CO_2 in N_2 at 16.5 mbar pressure. Here, we dilute a calibrated mixture of 5% CO_2 in N_2 (Linde Gas) with pure N_2 , down to 495 ppm, using two flow controllers. The measured spectrum is shown in Fig. 3 (in black, 500 averaged scans in ~ 16 min, 1.9 s per scan) alongside a fitted, modelled CO_2 spectrum (in red, inverted for clarity). The model spectrum is calculated using the HITRAN database parameters and a Voigt profile, convolved with a sinc function. The retrieved concentration from the fit is 485 ± 12 ppm. The uncertainty is calculated from the standard deviation of the noise in the residual of the fit. In Fig. 3a, the full rotational-vibrational band of CO_2 is shown. To demonstrate the agreement between the measurement and the fitting routine, an enlargement of the spectral features between 2357 cm^{-1} and 2363 cm^{-1} is displayed in Fig. 3b. The residuals are shown in the bottom panels (Fig. 3c,d). The rather featureless residuals demonstrate the high precision of the frequency calibration, as well as the good quality of the fitting routine. The small peaks which are still visible in the residual can be contributed to the influence of carbon dioxide in the beam path outside the

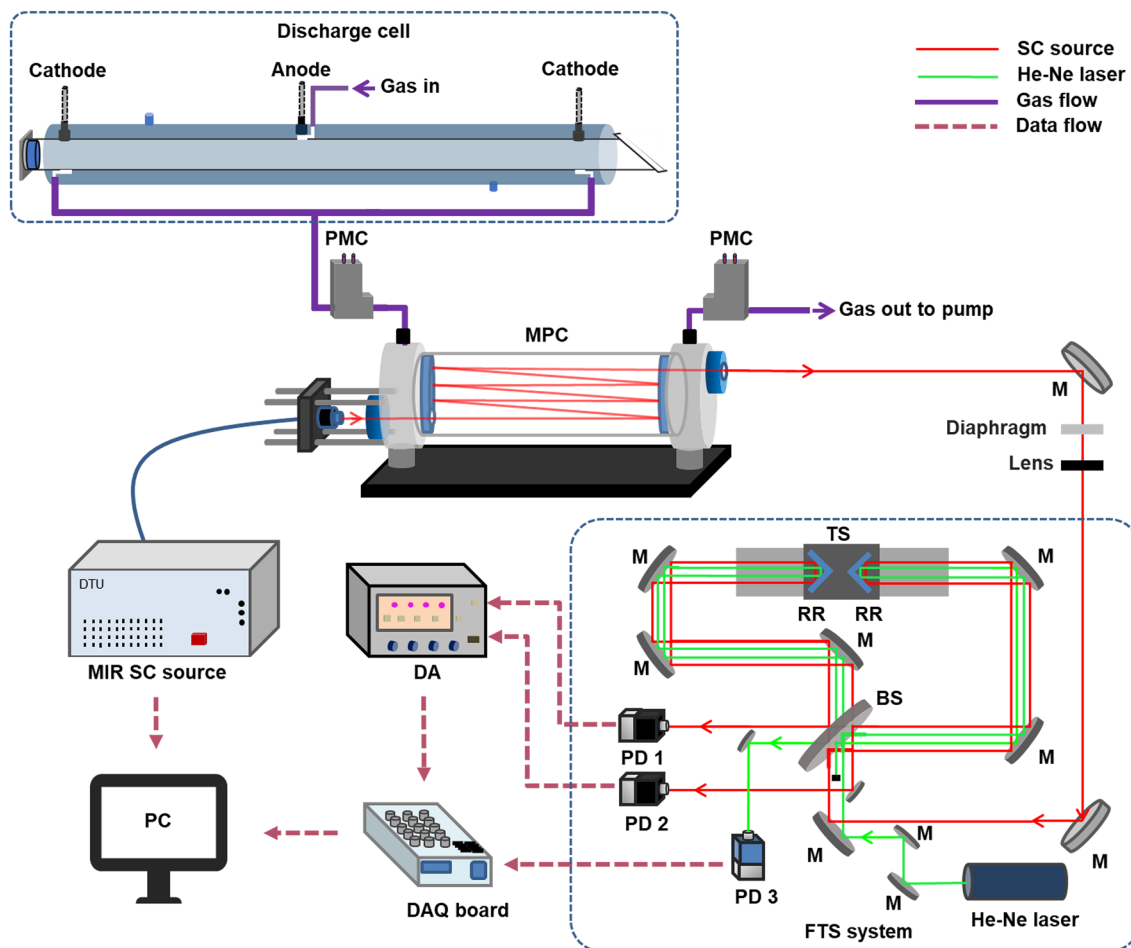


Figure 1. Experimental setup of the SC source and FTS-based multi-species detection system. *MPC* multipass cell, *PMC* pressure meter & controller, *M* mirror, *TS* translation stage, *RR* retroreflector mirror, *BS* beamsplitter, *He-Ne laser* helium–neon laser, *PD* photodetector, *DA* differential amplifier, *DAQ board* data acquisition board, *PC* computer.

MPC. The light intensity at these specific peaks is reduced in both the background and measurement spectrum to an extent that it degrades the fitting quality.

The linear response of the system to different applied CO_2 concentrations was evaluated in a dynamic range between 0.05% and 2.5% of CO_2 in N_2 , by diluting the 5% CO_2 in N_2 mixture further using pure N_2 gas. Each measurement consists of 500 averaged spectra, measured in ~ 16 min. The reference spectra for the linear fitting routine were simulated from the HITRAN database as described before. The retrieved concentrations from the fit versus the applied concentrations are shown in Fig. 4, together with the corresponding errors, exhibited in the lower panel. The linear fit shows a Pearson correlation coefficient square value of 0.9995, demonstrating a very good agreement between the measured concentration values and the applied concentrations. The corresponding relative errors are within a $\pm 4\%$ margin for the entire range, with an average error of 2%.

Product analysis of CO_2/N_2 plasmas. To further assess the performance of the system and to demonstrate its ability to quantify complex mixtures of reaction products, the outflow of a discharge was used. The discharge was generated in a flowing mixture of 50% CO_2 in N_2 (flow of 2 l_n/h) in a discharge cell at a pressure of 25 mbar. The applied voltage was 17.5 kV with a current of 10 mA that results in a specific energy input of 7.1 MJ/mol. The outflow of the discharge cell was guided to the *MPC*, which had a controlled pressure of 16.5 mbar. In Fig. 5, the measured absorbance spectra of nitrogen dioxide (NO_2), nitric oxide (NO), nitrous oxide (N_2O), CO , CO_2 and H_2O are shown (in black) together with corresponding simulated spectra (inverted, in color, using HITRAN parameters). The concentrations of the species retrieved from fitting the simulations to the absorption spectra are shown in Table 1. The practically featureless residual of the fit, shown in the bottom panel of Fig. 5, indicates a very good fit for all detected species. The few spikes which remain visible in the residual can be attributed to the effect of highly absorbing water vapor lines in the atmospheric air outside the *MPC*, degrading the fitting quality.

A wide variety of different species are detected over a range of concentration levels from hundreds of ppm to percentage-level. The broad spectral coverage does not only allow for detection of absorption lines of various

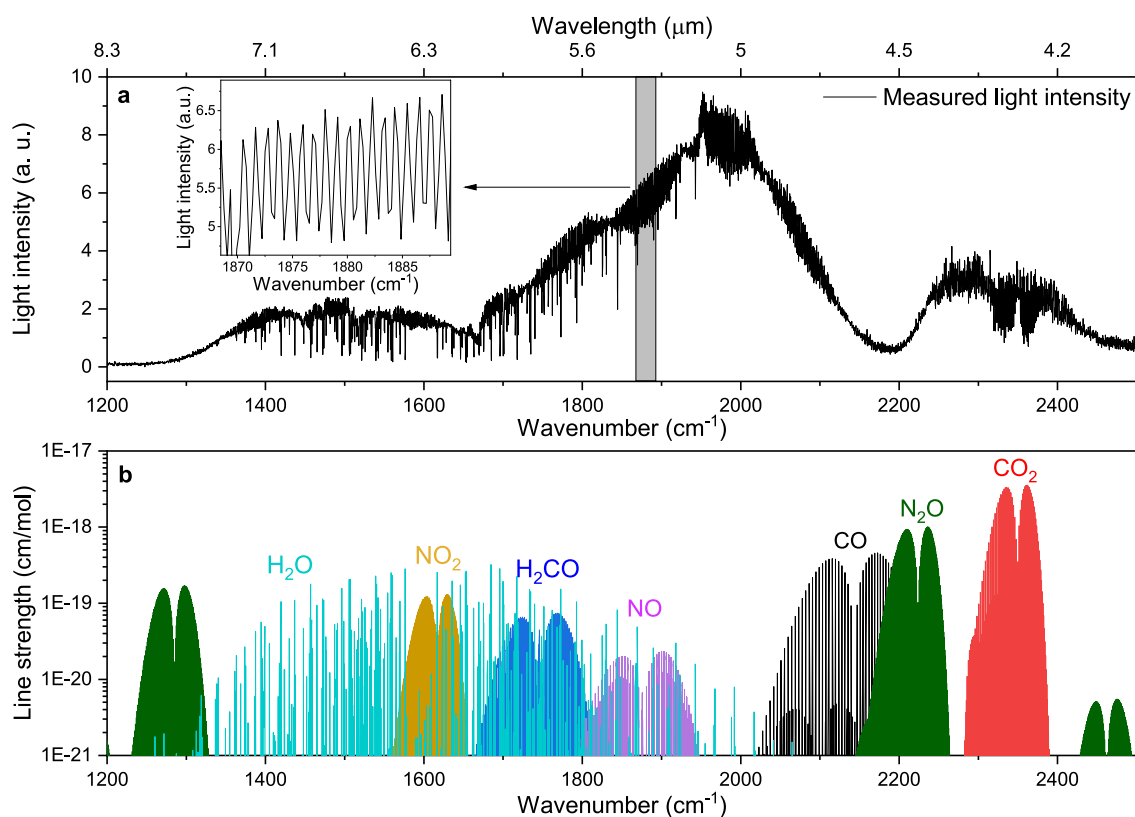


Figure 2. Spectral coverage of the MIR SC source and absorbing molecular species. (a) The spectrum of the MIR SC source with a spectral resolution of ~ 0.27 cm⁻¹ (8 GHz) measured under vacuum conditions, insert: an enlargement of the spectrum, showing the etalon fringes in the measured spectrum. (b) Simulated spectral line intensity of different species from HITRAN2020 between 1300 cm⁻¹ and 2500 cm⁻¹.

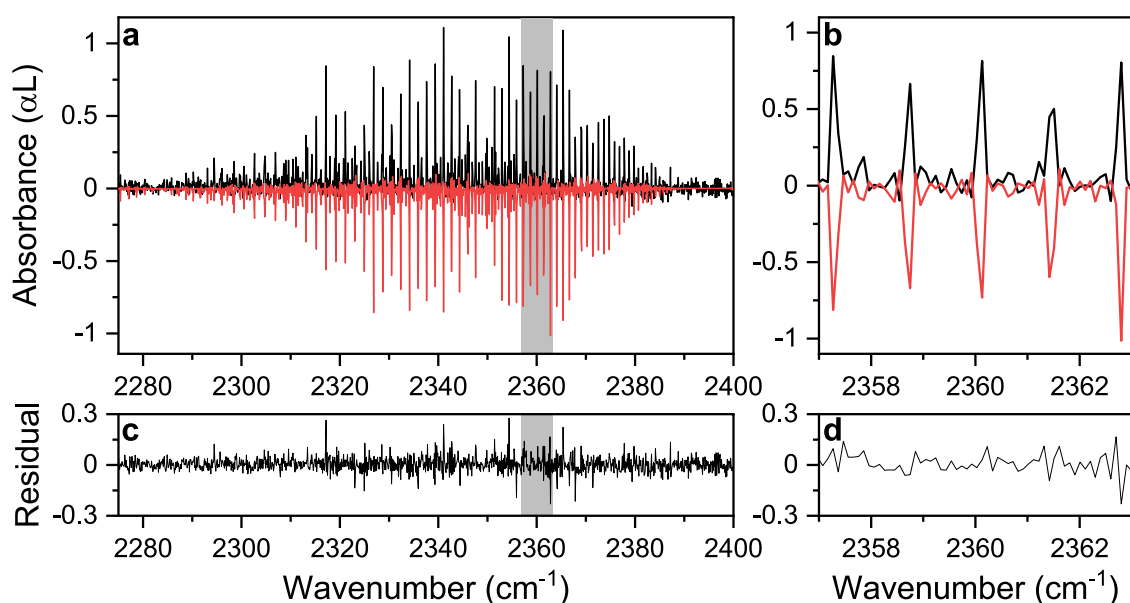


Figure 3. Experimental spectrum of CO₂. (a) Measured spectrum (in black, 0.1 cm⁻¹ spectral resolution, pressure 16.5 mbar, 500 averages in ~ 16 min) of 495 ppm CO₂ diluted in N₂ and a fitted modelled spectrum (in red, inverted) from the HITRAN database using a Voigt profile and convolved with a sinc-function. (b) Details of a part of the spectrum indicated in (a) as a grey rectangle. (c,d) Residual of the fit.

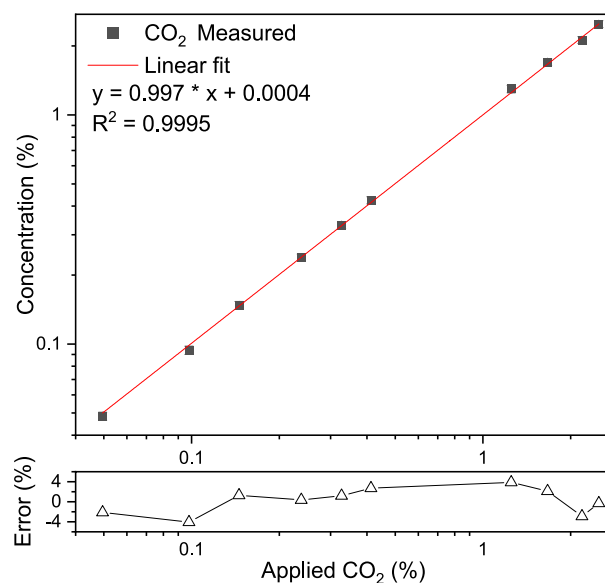


Figure 4. Retrieved concentrations of CO₂ for various dilutions of CO₂ in N₂, along with a linear fit to demonstrate the linear response of the system. The error provided is the relative difference between the applied and retrieved concentration.

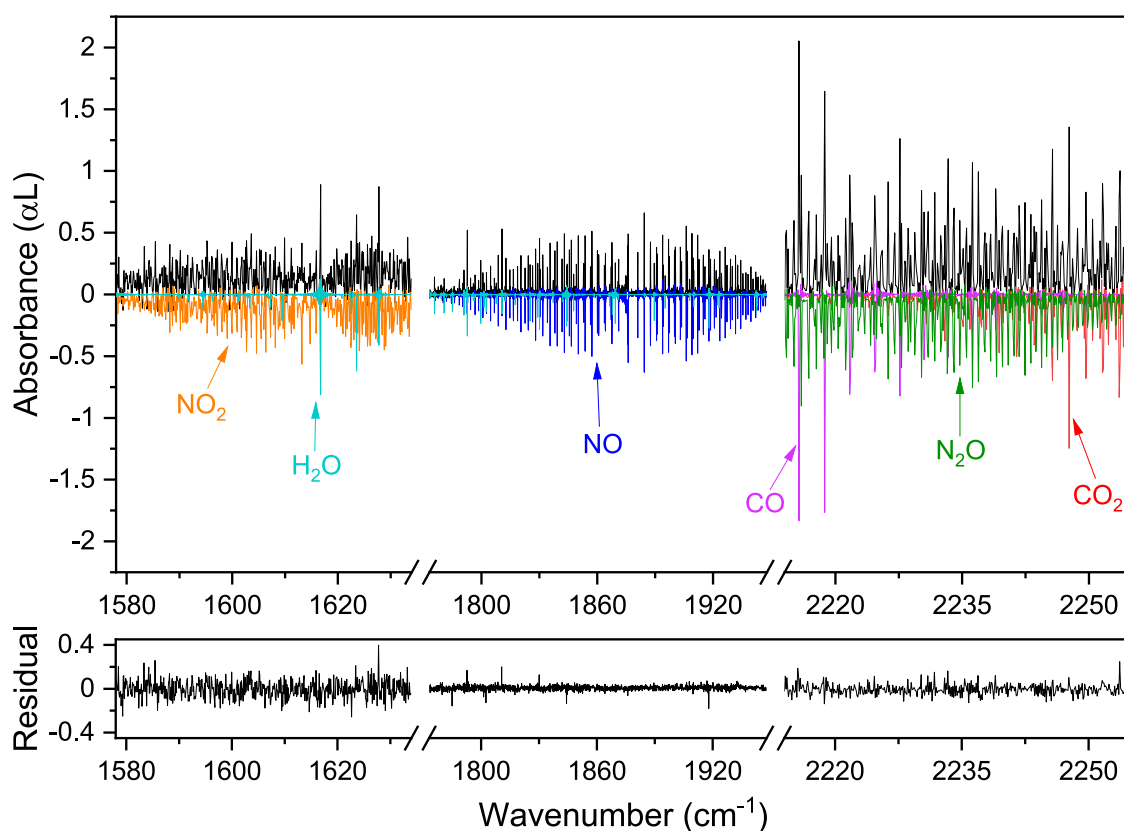


Figure 5. Measured spectrum (in black, 0.1 cm⁻¹ spectral resolution, 16.5 mbar pressure, ~ 16 min) of reaction products of a 50% CO₂/50% N₂ discharge and the fitted modelled spectra (in colors, inverted) based on the HITRAN database parameters and Voigt profiles convolved with a sinc function. The residual of the fit is shown in the lower panel.

	Retrieved concentration (% or ppm)	
	50% CO ₂ /50% N ₂	30% CO ₂ /70% CH ₄
Carbon dioxide (CO ₂)	13.0 ± 0.6%	13.9 ± 0.7%
Carbon monoxide (CO)	14.6 ± 0.7%	32.1 ± 1.7%
Nitrous oxide (N ₂ O)	570 ± 30 ppm	–
Nitrogen dioxide (NO ₂)	154 ± 13 ppm	–
Nitric oxide (NO)	0.33 ± 0.01%	–
Ethylene (C ₂ H ₄)	–	0.73 ± 0.03%
Formaldehyde (H ₂ CO)	–	0.13 ± 0.01%
Acetone (C ₃ H ₆ O)	–	0.3 ± 0.1%
Acetaldehyde (C ₂ H ₄ O)	–	0.3 ± 0.1%

Table 1. Retrieved concentrations of electric discharge products.

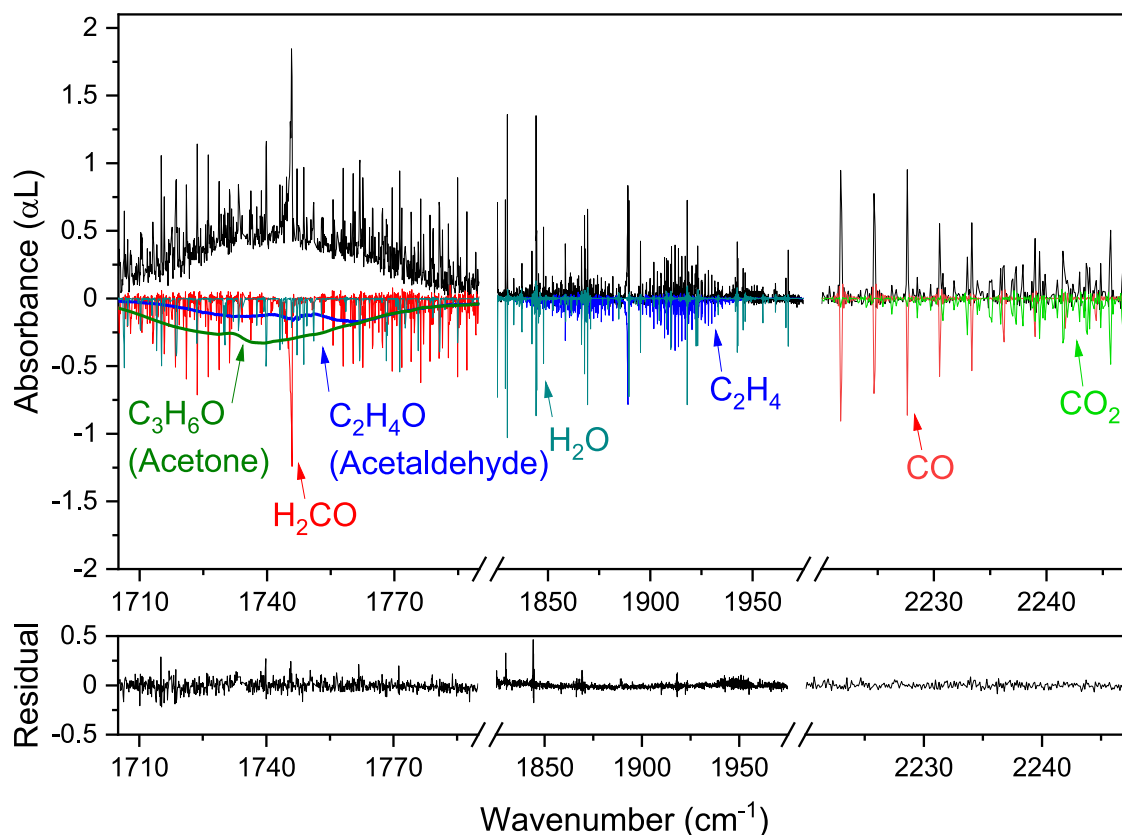


Figure 6. Measured spectrum of reaction products of a discharge of 70% CH₄ and 30% CO₂ (in black, 0.1 cm⁻¹ spectral resolution, 16.5 mbar pressure, ~ 16 min). Reference spectra of formaldehyde, water, carbon monoxide, carbon dioxide (from HITRAN), acetone and acetaldehyde (from PNNL) and ethylene (from GEISA) shown inverted.

compounds, but also to select absorption lines of a certain species with an appropriate line strength for the given concentration, preventing limitations arising from absorption lines which absorb almost 100% of the light.

Product analysis of CO₂/CH₄ plasmas. A bigger challenge for the spectroscopic analysis of a complex mixture of reaction products is the dry reforming of methane, as more complex molecules are formed, which cannot be found in HITRAN. Therefore, to extend the evaluation of the system, a CO₂/CH₄ discharge is generated. A discharge voltage of 18 kV with a current of 15 mA provided a specific energy input of 11 MJ/mol for a mixture of 70% CH₄ and 30% CO₂ (flow 2 l_n/h, 19 mbar pressure). The absorbance features of the detected products are presented in Fig. 6. Here, a broad absorbance feature is visible in the 1700–1800 cm⁻¹ wavenumber region. In general, this indicates the presence of molecular species with a large number of closely spaced rotational transitions in the vibrational band, which cannot be resolved spectroscopically at this pressure and tem-

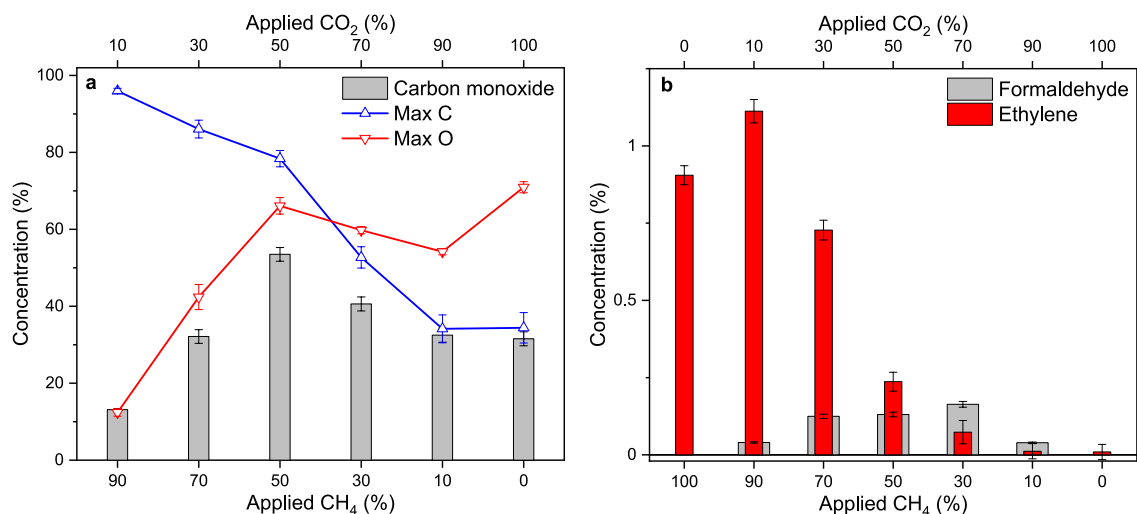


Figure 7. Retrieved concentrations of reaction products. **(a)** Measured CO concentrations for varying CH₄/CO₂ ratio generated by the plasma (in grey). Maximum amount of carbon atoms (Max C, blue) and oxygen atoms (Max O, red), available from the CO₂ and CH₄ depletion in the discharge, indicate the maximum CO concentration that can be generated. The measured CO-levels are below these values. **(b)** Measured concentrations of ethylene (in red) and formaldehyde (in grey) generated by the plasma for varying ratios of CH₄/CO₂.

perature. Using the PNNL database, this specific absorbance profile was found to be likely belonging to acetone (C₃H₆O) and acetaldehyde (C₂H₄O), both with a concentration of $0.3 \pm 0.1\%$. The concentration could however not be determined exactly, as PNNL is constructed with experimental data at 1 atmosphere pressure, which is significantly different from our experiment. We confirmed the presence of these two molecular species in our mixture using proton-transfer-reaction mass spectrometry (PTR-MS)⁴² and gas chromatography–mass spectrometry (GC–MS)⁴³. Moreover, the residual shows the ability of the system to detect overlapping absorbance features of multiple species, as both the acetone, acetaldehyde, formaldehyde (H₂CO) and most H₂O spectral features are fitted well with their reference spectra. Furthermore, the absorbance lines of ethylene (C₂H₄) around 1880 cm⁻¹ are not included in the HITRAN database. Therefore, the GEISA database⁴⁴ was used to create a simulated reference spectrum for C₂H₄, indicating a concentration of $0.73 \pm 0.03\%$.

In summary, this experiment demonstrates the system's ability to accurately detect numerous molecular species created in electric discharges of CO₂/CH₄, even for the ones with overlapping spectral features.

Plasmas with varying ratio of CO₂ and CH₄. To demonstrate the possibilities of the system for plasma analysis and study, a quantitative analysis of the products formed in the electric discharge is made, using a series of measurements with a varying CO₂/CH₄ ratio (gas flow 2 l_n/h, 18 kV, 15 mA, specific energy input of 11 MJ/mol). In Fig. 7a, the measured CO concentration is displayed for varying mixtures of CO₂/CH₄, along with the assumed limit in CO production, calculated from the number of carbon (in red) and oxygen atoms (in blue) available in the system to react to CO. These limits are calculated from the retrieved CO₂ concentrations, which are shown in Supplementary Fig. 1. From the difference between the CO₂ concentrations with the discharge on or off, the maximum number of carbon and oxygen atoms available for conversion is determined. The highest CO production is found for a 50/50-mixture of CO₂/CH₄. The CO values are within the expected maximum available carbon and oxygen atoms generated in the plasma, indicating a correct reaction balance. As the concentration of CO (~53%) is higher than the concentration of converted CO₂, this indicates that CO is not only formed by removal of an oxygen atom from CO₂, but also by recombination of the removed oxygen atom from CO₂ with a dehydrogenated carbon atom from CH₄. Furthermore, there is additional production of C₂H₄ and H₂CO (Fig. 6), of which the retrieved concentrations are presented in Fig. 7b.

Discussion

A MIR SC FTS system is presented for the first time for plasma analysis. We showed that various molecular species of interest can be detected and quantified across the spectral range of the supercontinuum source, while the high spectral resolution from the FTS allowed for identification of molecular species with overlapping absorption features. Therefore, the MIR SC FTS system provides a unique set of characteristics that are especially useful for plasma diagnosis, combining the broad spectral coverage, high spectral power, and high spectral resolution with a high spatial coherence, stability and ease of use. The high detection sensitivity makes it possible to monitor the molecular reaction products in a low-pressure plasma, minimizing spectral interference between different species and accurately determining their concentrations.

A rather detailed comparison of the MIR SC FTS with other spectroscopy systems in the MIR range is presented in our previous work³⁵. The noise equivalent absorption sensitivity of the MIR SC FTS is one to two

orders of magnitude lower than MIR optical frequency comb-based spectrometers and it also provides coarser spectral resolution compared to comb-based systems. However, the broader spectral coverage of the MIR SC FTS allows simultaneous detection of a large number of molecular species. In addition, the ease-of-use, compactness, robustness, and lower cost of MIR SC sources make them better suited for real-life plasma applications.

Classical FTIRs can match the spectral coverage of our system. As mentioned elsewhere³⁵, they currently provide a better Noise Equivalent Absorption Sensitivity compared to the MIR SC FTS presented here. However, classical FTIRs tend to operate at a lower spectral resolution, as the combination of high resolution with the relatively low spectral power density of a thermal source would increase the need for spectral averaging and consequently lengthen the measurement time. Most importantly, the thermal sources lack spatial coherence, making it challenging to create long interaction path lengths (e.g. by using an MPC with a long effective path length) to maximize the sensitivity. Furthermore, a well-collimated beam with a small beam diameter is required for in-situ monitoring in long (> 1 m) plasma cells, which is also difficult to obtain using thermal sources.

Our system's performance can also be compared specifically to previous studies on plasma analysis using QCLs²⁰ and tunable diode lasers¹⁴, which are currently the most frequently used laser-based systems for absorption spectroscopy on plasmas. Their narrow spectral range, which generally is in the order of a few wavenumbers (with some exceptions for external cavity QCLs), limits the number of detectable molecular species as well as the detection and identification of unknown compounds and introduces difficulties for overlapping/broadband spectra. For instance, detection, identification, and quantification of the overlapping spectra of acetaldehyde, acetone, and formaldehyde as in Fig. 6 would have been significantly more difficult with such a system.

In conclusion, the reaction products were quantified for a plasma with a varying ratio of CO₂ and CH₄. The CO yield was found to increase when CH₄ was added to the CO₂ plasma, which could be explained by the recombination of the removed oxygen atom from CO₂ with a dehydrogenated carbon atom from CH₄. The observed trends in the generation of the other observed products, H₂CO and C₂H₄, demonstrated a good agreement with previous studies. H₂CO should be composed from H-atoms of CH₄ and O-atoms of CO₂ and is indeed only found in mixtures containing both CH₄ and CO₂⁴⁵. The formation of C₂H₄ increases towards higher concentrations of CH₄ in the mixture and can be easily explained as C₂H₄ is a product from the dehydrogenation of CH₄⁴⁶.

Currently, the relative intensity noise of the MIR SC source limits the sensitivity of the spectrometer, although this is not essential for the demonstrated application, in identification and quantification of the products of a plasma reaction. Moreover, with the current rapid developments in MIR SC sources, it is anticipated that the intensity noise of these sources will be reduced further in the near future^{29,34}. Finally, the spatial coherence of the MIR SC beam could also be exploited for other applications, such as for accurate in-situ probing in plasmas, to monitor the plasma dynamics, as well as to detect intermediate products in the plasma.

Finally, besides the application of this system for electrolytic chemical conversions, it can potentially be applied as a spectroscopic tool for many more plasma applications. For example, within the synthesis of carbon nanotubes using plasma-enhanced chemical vapor deposition (PECVD), monitoring a correct flow of reactants and the formation of gas phase intermediates and products is currently done with mass spectrometry⁴⁷. Our system could replace mass spectrometry, providing on-line measurements and being able to distinguish species with identical masses. Furthermore, in plasma medicine cold atmospheric plasma jets are used to treat human skin or wounds⁴⁸. Optical Emission Spectroscopy (OES) and FTIR are used to investigate the species formed in these plasmas. As OES lacks quantification⁴⁹ and FTIR lacks sensitivity due to limited interaction lengths and spectral resolution⁵⁰, a MIR SC FTS system might be preferred to quantify the species formed in plasma jets for these applications. Similarly, the system could be of interest for other plasma-based techniques, such as wastewater treatment⁵¹, or surface and material modification and sterilization^{52,53}.

Methods

Fourier transform spectrometer. The overview of the full experimental system is presented in Fig. 1. The output fiber of the MIR SC source is connected to a reflective collimator that is mounted on the MPC to limit the optical path outside the MPC. After passing through the MPC, the MIR SC beam is aligned to the Fourier transform spectrometer (FTS) using two flat mirrors. A diaphragm is used to filter stray light and a long-focal-point lens was used to match the beam waist to the center of the translation stage in the FTS. The setup of the FTS system has been described in detail in our previous work³⁵. Briefly, the FTS system is based on a Michelson interferometer; the incoming light beam is split by a beamsplitter into two arms, each leading to a hollow retroreflector mirror. The retroreflector mirrors reflect the beams with slight horizontal and vertical shifts, so that the reflected beams recombine on the beamsplitter and the two resulting superpositions of the beams (interfering pair of beams) can both propagate towards separate photovoltaic detectors (PVI-4TE-10.6, Vigo Systems). The two interference patterns at the output of the detectors are subtracted from each other by a differential amplifier (SR560, Stanford Research system) in a balanced detection scheme. Since the two interference patterns are out-of-phase, but the intensity noise is in-phase, the balanced detection scheme highly reduces intensity noise, which leads to an effective improvement of the signal-to-noise ratio (SNR). The two retroreflectors are mounted back-to-back on a linear-motor translator stage. Scanning the translator stage over a distance of 2.5 cm results in an optical path difference of 10 cm between the two beams, which provides a spectral resolution of 0.1 cm⁻¹ (3 GHz). A He–Ne laser beam is sent along the SC beam path in the FTS to create an interferogram for a known and stable wavelength. The interferogram of the He–Ne laser is recorded by a separate photovoltaic detector. To prevent the interference of absorption by H₂O and CO₂ in the ambient air with the measurement, the FTS is confined in a closed box and continuously purged with N₂ gas.

Data analysis. For real-time analysis of the detected interferograms, a LabVIEW-based data processing system is developed. A flowchart of the algorithms used for this analysis is shown in Supplementary Fig. 2.

The wavenumber calibration of the MIR SC source is performed through a resampling process using a He–Ne laser. In this process, explained in detail in Ref.³⁵, the algorithm finds the zero-crossings of the He–Ne laser interferogram (whose beam is propagating in parallel to the MIR SC beam) by linear interpolation. Then, it linearly interpolates the MIR SC interferogram at the zero-crossing positions of the He–Ne laser interferogram. Therefore, the interpolated MIR SC interferogram in the zero-crossing domain is calibrated with an optical path difference step size equal to the zero-crossing intervals. After the calibration, a Fast Fourier Transform (FFT) of the resampled interferograms yields the spectra. Note that we used a natural boxcar apodization function for the interferograms. The absorbance spectrum is obtained by dividing the transmission spectrum of the sample to the background (the latter is taken after purging the MPC with pure N₂ gas) and taking the natural logarithm. The absorbance spectra of the different species are simulated, using parameters from the HITRAN2020⁴¹ or GEISA⁴⁴ database and convoluted with a sinc instrument lineshape function, to fit the natural boxcar apodization of the interferograms. GEISA was used to simulate the absorbance of ethylene (C₂H₄) around 1900 cm⁻¹, since this ethylene band is not completely included in HITRAN. The PNNL⁵⁴ database was used to identify absorbance from acetone (C₃H₆O) and acetaldehyde (C₂H₄O). However, PNNL contains actual FTIR measurements of absorbance spectra at atmospheric pressure, which cannot correctly be recalculated for low pressures. Finally, the concentrations of different species are calculated using a multiple linear regression algorithm based on the least squares method³⁵. Given the limitations of the PNNL data, the concentration of acetone and acetaldehyde can only be approximated.

Plasma conditions. For the generation of the plasma, a water-cooled discharge tube (length 180 cm, internal diameter of 1.5 cm) is used to create a uniform electric discharge. The anode and gas inlet are located in the center, while two hollow cathodes (4 cm long each) and the gas outlets are located at either end of the discharge tube. A current-stabilized high-voltage (HV) power supply (Haefely Hipotronics, US, providing up to 25 kV, 40 mA) is used for generating a direct current (DC) electric discharge in the tube²². The gas inflow is regulated with flow controllers and the pressure inside the discharge tube is regulated with a back-pressure controller (25 mbar). The outflow of the gas from the discharge tube is directed to a MPC (effective path length of 31.2 m), which is regulated by another back-pressure controller to a pressure lower than in the discharge tube (16.5 mbar) to ensure a proper gas flow.

Data availability

The data that support the findings of this study are available from the corresponding authors on reasonable request.

Received: 14 March 2022; Accepted: 27 May 2022

Published online: 10 June 2022

References

- Snoeckx, R. & Bogaerts, A. Plasma technology: A novel solution for CO₂ conversion?. *Chem. Soc. Rev.* **46**, 5805–5863 (2017).
- Lebouvier, A., Iwarere, S. A., D'Argenlieu, P., Ramjugernath, D. & Fulcheri, L. Assessment of carbon dioxide dissociation as a new route for syngas production: A comparative review and potential of plasma-based technologies. *Energy Fuels* **27**, 2712–2722 (2013).
- Xia, Y. *et al.* Combined steam and CO₂ reforming of CH₄ for syngas production in a gliding arc discharge plasma. *J. CO₂ Util.* **37**, 248–259 (2020).
- Westermann, A. *et al.* Insight into CO₂ methanation mechanism over NiUSY zeolites: An operando IR study. *Appl. Catal. B* **174–175**, 120–125 (2015).
- Fan, M.-S., Abdullah, A. Z. & Bhatia, S. Catalytic technology for carbon dioxide reforming of methane to synthesis gas. *Chem-CatChem* **1**, 192–208 (2009).
- Pakhare, D. & Spivey, J. A review of dry (CO₂) reforming of methane over noble metal catalysts. *Chem. Soc. Rev.* **43**, 7813–7837 (2014).
- Liu, S., Winter, L. R. & Chen, J. G. Review of plasma-assisted catalysis for selective generation of oxygenates from CO₂ and CH₄. *ACS Catal.* **10**, 2855–2871 (2020).
- Li, D. *et al.* CO₂ reforming of CH₄ by atmospheric pressure glow discharge plasma: A high conversion ability. *Int. J. Hydrog. Energy* **34**, 308–313 (2009).
- Paulmier, T. & Fulcheri, L. Use of non-thermal plasma for hydrocarbon reforming. *Chem. Eng. J.* **106**, 59–71 (2005).
- Bogaerts, A. & Neyts, E. C. Plasma technology: An emerging technology for energy storage. *ACS Energy Lett.* **3**, 1013–1027 (2018).
- Tao, X. *et al.* CH₄–CO₂ reforming by plasma: Challenges and opportunities. *Prog. Energy Combust. Sci.* **37**, 113–124 (2011).
- Puliyalil, H., Lašič Jurković, D., Dasireddy, V. D. B. C. & Likozar, B. A review of plasma-assisted catalytic conversion of gaseous carbon dioxide and methane into value-added platform chemicals and fuels. *RSC Adv.* **8**, 27481–27508 (2018).
- Xu, S. *et al.* CO poisoning of Ru catalysts in CO₂ hydrogenation under thermal and plasma conditions: A combined kinetic and diffuse reflectance infrared Fourier transform spectroscopy-mass spectrometry study. *ACS Catal.* **10**, 12828–12840 (2020).
- Röpcke, J., Lombardi, G., Rousseau, A. & Davies, P. B. Application of mid-infrared tuneable diode laser absorption spectroscopy to plasma diagnostics: A review. *Plasma Sources Sci. Technol.* **15**, S148–S168 (2006).
- Azzolina-Jury, F. & Thibault-Starzyk, F. mechanism of low pressure plasma-assisted CO₂ hydrogenation over Ni-USY by micro-second time-resolved FTIR spectroscopy. *Top. Catal.* **60**, 1709–1721 (2017).
- Horvth, G., Skaln, J. D. & Mason, N. J. FTIR study of decomposition of carbon dioxide in dc corona discharges. *J. Phys. D: Appl. Phys.* **41**, 225207 (2008).
- Damen, M. A., Martini, L. M. & Engeln, R. Temperature evolution in a pulsed CO₂-N₂ glow discharge measured using quantum cascade laser absorption spectroscopy. *Plasma Sources Sci. Technol.* **29**, 065016 (2020).
- Marinov, D. *et al.* Surface vibrational relaxation of N₂ studied by CO₂ titration with time-resolved quantum cascade laser absorption spectroscopy. *J. Phys. D: Appl. Phys.* **45**, 175201 (2012).
- Welzel, S. *et al.* Quantum cascade laser absorption spectroscopy as a plasma diagnostic tool: An overview. *Sensors* **10**, 6861–6900 (2010).
- Röpcke, J., Davies, P. B., Lang, N., Rousseau, A. & Welzel, S. Applications of quantum cascade lasers in plasma diagnostics: A review. *J. Phys. D: Appl. Phys.* **45**, 423001 (2012).

21. Abbas, M. A. *et al.* Broadband time-resolved absorption and dispersion spectroscopy of methane and ethane in a plasma using a mid-infrared dual-comb spectrometer. *Sensors* **20**, 6831 (2020).
22. Abbas, M. A. *et al.* Time-resolved mid-infrared dual-comb spectroscopy. *Sci. Rep.* **9**, 17247 (2019).
23. Dębek, R., Azzolina-Jury, F., Travert, A., Mauge, F. & Thibault-Starzyk, F. Low-pressure glow discharge plasma-assisted catalytic CO₂ hydrogenation: The effect of metal oxide support on the performance of the Ni-based catalyst. *Catal. Today* **337**, 182–194 (2019).
24. Vasilyev, S. *et al.* Super-octave longwave mid-infrared coherent transients produced by optical rectification of few-cycle 25-μm pulses. *Optica* **6**, 111–114 (2019).
25. Petersen, C. R. *et al.* Mid-infrared supercontinuum covering the 1.4–13.3 μm molecular fingerprint region using ultra-high NA chalcogenide step-index fibre. *Nat. Photonics* **8**, 830–834 (2014).
26. Petersen, C. R., Moselund, P. M., Huot, L., Hooper, L. & Bang, O. Towards a table-top synchrotron based on supercontinuum generation. *Infrared Phys. Technol.* **91**, 182–186 (2018).
27. Wang, Y. *et al.* Mid-infrared supercontinuum generation spanning from 1.9 to 5.7 μm in a chalcogenide fiber taper with ultra-high NA. *Infrared Phys. Technol.* **88**, 102–105 (2018).
28. Kwarkye, K. *et al.* In-amplifier and cascaded mid-infrared supercontinuum sources with low noise through gain-induced soliton spectral alignment. *Sci. Rep.* **10**, 8230 (2020).
29. Sylvestre, T. *et al.* Recent advances in supercontinuum generation in specialty optical fibers [Invited]. *J. Opt. Soc. Am. B* **38**, F90 (2021).
30. Eslami Jahromi, K. *et al.* Sensitive multi-species trace gas sensor based on a high repetition rate mid-infrared supercontinuum source. *Opt. Express* **28**, 26091–26101 (2020).
31. Kilgus, J., Duswald, K., Langer, G. & Brandstetter, M. Mid-infrared standoff spectroscopy using a supercontinuum laser with compact Fabry-Pérot filter spectrometers. *Appl. Spectrosc.* **72**, 634–642 (2018).
32. Israelsen, N. M. *et al.* Real-time high-resolution mid-infrared optical coherence tomography. *Light* **8**, 11 (2019).
33. Zorin, I. *et al.* Mid-infrared Fourier-domain optical coherence tomography with a pyroelectric linear array. *Opt. Express* **26**, 33428–33439 (2018).
34. Zorin, I., Gattinger, P., Ebner, A. & Brandstetter, M. Advances in mid-infrared spectroscopy enabled by supercontinuum laser sources. *Opt. Express* **30**, 5222–5254 (2022).
35. Abbas, M. A. *et al.* Fourier transform spectrometer based on high-repetition-rate mid-infrared supercontinuum sources for trace gas detection. *Opt. Express* **29**, 22315–22330 (2021).
36. Petersen, C. R. *et al.* Mid-infrared multispectral tissue imaging using a chalcogenide fiber supercontinuum source. *Opt. Lett.* **43**, 999–1002 (2018).
37. Kilgus, J. *et al.* Diffraction limited mid-infrared reflectance microspectroscopy with a supercontinuum laser. *Opt. Express* **26**, 30644–30654 (2018).
38. Napier, B. *et al.* Ultra-broadband infrared gas sensor for pollution detection: The TRIAGE project. *J. Phys. Photonics* **3**, 031003 (2021).
39. Durocher-Jean, A., Jean-Ruel, H., Dion-Bertrand, L. I., Blais-Ouellette, S. & Stafford, L. Ultra-high-resolution optical absorption spectroscopy of DC plasmas at low pressure using a supercontinuum laser combined with a laser line tunable filter and a HyperFine spectrometer. *J. Phys. D: Appl. Phys.* **54**, 085204 (2021).
40. Woyessa, G. *et al.* Power stable 1.5–10.5 μm cascaded mid-infrared supercontinuum laser without thulium amplifier. *Opt. Lett.* **46**, 1129–1132 (2021).
41. Gordon, I. E. *et al.* The HITRAN2020 molecular spectroscopic database. *J. Quant. Spectrosc. Radiat. Transfer* **277**, 107949 (2022).
42. Danner, H., Samudrala, D., Cristescu, S. M. & van Dam, N. M. Tracing Hidden Herbivores: Time-Resolved Non-Invasive Analysis of Belowground Volatiles by Proton-Transfer-Reaction Mass Spectrometry (PTR-MS). *J. Chem. Ecol.* **38**, 785–794 (2012).
43. Sola Martínez, R. A. *et al.* Data preprocessing workflow for exhaled breath analysis by GC/MS using open sources. *Sci. Rep.* **10**, 22008 (2020).
44. Delahaye, T. *et al.* The 2020 edition of the GEISA spectroscopic database. *J. Mol. Spectrosc.* **380**, 111510 (2021).
45. Kozlov, K. V., Michel, P. & Wagner, H. E. Synthesis of organic compounds from mixtures of methane with carbon dioxide in dielectric-barrier discharges at atmospheric pressure. *Plasmas Polym.* **5**, 129–150 (2000).
46. Delikonstantis, E., Scapinello, M. & Stefanidis, G. D. Low energy cost conversion of methane to ethylene in a hybrid plasma-catalytic reactor system. *Fuel Process. Technol.* **176**, 33–42 (2018).
47. Nozaki, T. & Okazaki, K. Carbon nanotube synthesis in atmospheric pressure glow discharge: A review. *Plasma Process. Polym.* **5**, 300–321 (2008).
48. Fridman, G. *et al.* Applied plasma medicine. *Plasma Process. Polym.* **5**, 503–533 (2008).
49. Winter, J. *et al.* Feed gas humidity: A vital parameter affecting a cold atmospheric-pressure plasma jet and plasma-treated human skin cells. *J. Phys. D: Appl. Phys.* **46**, 295401 (2013).
50. Schmidt-Bleker, A. *et al.* Reactive species output of a plasma jet with a shielding gas device—combination of FTIR absorption spectroscopy and gas phase modelling. *J. Phys. D: Appl. Phys.* **47**, 145201 (2014).
51. Wang, X., Zhou, M. & Jin, X. Application of glow discharge plasma for wastewater treatment. *Electrochim. Acta* **83**, 501–512 (2012).
52. Ren, J., Yao, M., Yang, W., Li, Y. & Gao, J. Recent progress in the application of glow-discharge electrolysis plasma. *Cent. Eur. J. Chem.* **12**, 1213–1221 (2014).
53. Samanta, K., Jassal, M. & Agrawal, A. K. Atmospheric pressure glow discharge plasma and its applications in textile. *Indian J. Fibre Text. Res.* **31**, 83–98 (2006).
54. Sharpe, S. W. *et al.* Gas-phase databases for quantitative infrared spectroscopy. *Appl. Spectrosc.* **58**, 1452–1461 (2004).

Acknowledgements

The authors would like to thank Dr. Joris Meurs for performing the PTR-MS and GC-MS measurements. Ningwu Liu is supported by China Scholarship Council funding (CSC, 202006500008).

Author contributions

G.W., C.R.P. and O.B. developed the SC source at DTU Fotonik; R.K., N.L., K.E.J., M.N., F.J.M.H. and A.K. developed the FTS; R.K., N.L., F.J.M.H., A.K. and S.M.C. conceptualized the experiments; R.K., N.L., G.v.R., F.J.M.H., A.K. and S.M.C. provided interpretation of the plasma results; R.K. and N.L. performed the experiments, analyzed the experimental data, wrote the initial manuscript and contributed equally to this work; All authors reviewed the manuscript.

Funding

EU H2020-ICT-37 (TRIAGE project, 101015825), EU H2020-ICT-2016-1 (FLAIR project, 732968). Ningwu Liu is supported by China Scholarship Council funding (CSC, 202006500008).

Competing interests

The authors declare no direct financial relationship between the companies NKT and NORBLIS and the academic institutes that developed the FTS and performed the plasma experiments, and that the companies did not directly fund this study/manuscript. The SC source was developed in the framework of the EU H2020 programme (FLAIR project, 732968). The development of the FTS instrument and reporting of the results were carried out by the authors at Radboud University, independent of the institute that manufactured the SC source.

Additional information

Supplementary Information The online version contains supplementary material available at <https://doi.org/10.1038/s41598-022-13787-w>.

Correspondence and requests for materials should be addressed to A.K.

Reprints and permissions information is available at www.nature.com/reprints.

Publisher's note Springer Nature remains neutral with regard to jurisdictional claims in published maps and institutional affiliations.



Open Access This article is licensed under a Creative Commons Attribution 4.0 International License, which permits use, sharing, adaptation, distribution and reproduction in any medium or format, as long as you give appropriate credit to the original author(s) and the source, provide a link to the Creative Commons licence, and indicate if changes were made. The images or other third party material in this article are included in the article's Creative Commons licence, unless indicated otherwise in a credit line to the material. If material is not included in the article's Creative Commons licence and your intended use is not permitted by statutory regulation or exceeds the permitted use, you will need to obtain permission directly from the copyright holder. To view a copy of this licence, visit <http://creativecommons.org/licenses/by/4.0/>.

© The Author(s) 2022